AIAA JOURNAL
Vol. 40, No. 4, April 2002

Body–Vortex Interaction, Sound Generation, and Destructive Interference

Hsiao C. Kao*
NASA John H. Glenn Research Center at Lewis Field, Cleveland, Ohio 44135

It is generally recognized that the interaction of vortices with downstream blades is a major source of noise production. To analyze this problem numerically, a two-dimensional model of inviscid flow, together with the method of matched asymptotic expansions, is proposed. The method of matched asymptotic expansions is used to match the inner region of incompressible flow to the outer region of compressible flow. Because of incompressibility, relatively simple numerical methods are available to treat multiple vortices and multiple bodies of arbitrary shape. Disturbances from these vortices and bodies propagate outward as sound waves. Because of their interactions, either constructive or destructive interference may result. When it is destructive, the combined sound intensity can be reduced, sometimes substantially.

Introduction

INTERACTION of rotor tip vortices with downstream stators or other blades is commonly regarded as an important source of noise production.[1–3] Although it is difficult to separate vortices from other secondary flow effects, the notion that vortices play an important role is generally accepted. To make the problem tractable, a two-dimensional model with rectilinear vortices in an inviscid flow is proposed. The cases to be considered are a moving vortex interacting with a single body (blade) and with several bodies and several moving vortices interacting with several bodies. Because the trailing-edge condition will be imposed, wakes behind the blades are expected to occur.

The main assumption made here is that the bodies must be acoustically compact. In other words, the Mach number must be relatively low. This enables us to use the method of asymptotic expansions to match the inner solution, which is incompressible, with the outer solution, which is compressible and satisfies the acoustic equation. Because several bodies may be present, both constructive and destructive interference of sound waves from neighboring bodies have to be considered. By manipulation of the interference, it is possible to achieve pressure attenuation and reduce sound intensity.

Under the assumption of low Mach number, the characteristic length of the body is, in general, much smaller than the acoustic wavelength, which implies that the compactness ratio is small and the flow in the vicinity of the body is not wavelike. Dowling and Ffowcs Williams[4] stated that all acoustic motions in the vicinity of a singularity are solutions of Laplace's equations. In the present investigation, a body is represented by surface vorticity elements. Therefore, the inner region surrounding the body is incompressible and is governed by the Laplace equation. Disturbances generated in this region propagate outward as acoustic signals. Thus, the outer region is compressible and governed by the acoustic equation.

Since the pioneer work of Lighthill, the acoustic analogy has been the basis of other methods. For low Mach number flows, Crow's discussion[5] showed rigorously that source terms in the acoustic analogy can be separated from the acoustic far field, and these terms are the incompressible part of the near field. Since then, using asymptotic matching to solve aeroacoustic problems in low-speed flows has been conducted recurrently.[6–13] In these studies, if a body is present, it is usually of simple shape and amenable to conformal mapping. Here, this method is broadened to include multiple bodies of arbitrary shape. With this extension, interference of neighboring bodies can be studied.

The time scale for blade–vortex interaction is of the order of $\bar{L}/\bar{U}_0$, where $\bar{L}$ is the length of the body and $\bar{U}_0$ is the freestream velocity. In this time interval, an acoustic wave has propagated to the distance of $\bar{L}/M_0$, which is much larger than $\bar{L}$ as M_0, the freestream Mach number, approaches to zero. Thus, there are two disparate lengths, an indication of a singular perturbation problem.[14]

The advantage of this approach lies mostly in the inner region, where incompressible solutions for several bodies can be obtained readily by a number of numerical methods. The method chosen here is Martensen's surface vorticity method. This method, which has been thoroughly investigated by Lewis,[15] is convenient for the present purpose because the surface is replaced by vorticity elements, which, along with moving vortices, can be treated similarly by the Biot–Savart law.

The acoustic equation in the outer region, after the Fourier transform, becomes a Bessel equation, whose outgoing wave is represented by a Hankel function. Therefore, none of the unresolved complications in computational aeroacoustics appear. The remaining task is to match the two regions and to perform the inverse Fourier transform to return to the physical space.

Method of Validation

To gain confidence in using asymptotic matching to solve aeroacoustic problems, a simple problem of acoustic radiation by an oscillating circular cylinder is first examined. In this case, a term-by-term comparison between the analytical and asymptotic solutions can be made without recourse to numerical results. Although this is a simple example, the matching procedures for more complicated problems are the same. Therefore, more details than necessary are given in the following to lessen explanations for vortex interaction problems later.

Inner Solution and Its Fourier Transform

The motion of an oscillating circular cylinder is expressed as $\bar{U}_C \exp(i\bar{\omega}_C\bar{t})$, whose normal component on the surface is $\bar{U}_C \exp(i\bar{\omega}_C\bar{t})\cos\theta$. Thus, the velocity potential is

$$\bar{\phi} = -\bar{U}_C(\bar{a}^2/\bar{r})\exp(i\bar{\omega}_C\bar{t})\cos\theta$$

where $\bar{U}_C$ is the amplitude of oscillating velocity, $\bar{a}$ the radius of the cylinder, $\bar{\omega}_C$ the angular frequency, $\bar{r}$ the radial distance, $\bar{c}$ the speed of sound, and $\bar{t}$ the time. For small oscillations, the linearized Bernoulli equation is valid and gives the perturbed pressure in the inner region as

Received 27 January 2001; revision received 28 September 2001; accepted for publication 1 October 2001.

*Aerospace Engineer, Nozzle Branch, retired; current address: P. O. Box 360872, Strongsville, OH 44136.

$$p_i' = -\frac{\partial \phi}{\partial t} = \frac{i\omega_C M_C}{R}\cos\theta \exp(i\omega_C t) \tag{1}$$

The symbols in this equation refer to dimensionless quantities and are defined as follows:

$$p_i' = \bar{p}'/\bar{\rho}_0 \bar{U}_C^2, \qquad \phi = \bar{\phi}/\bar{U}_C \bar{a}, \qquad \omega_C = \bar{\omega}_C \bar{a}/\bar{U}_C$$
$$r = \bar{r}/\bar{a}, \qquad R = M_C r, \qquad M_C = \bar{U}/\bar{c}, \qquad t = \bar{t}\bar{U}_C/\bar{a}$$

By application of the Fourier transform pair to Eq. (1),

$$\hat{f}(R,\omega) = \int_{-\infty}^{\infty} f(R,t) e^{-i\omega t}\, \mathrm{d}t$$
$$f(R,t) = \frac{1}{2\pi}\int_{-\infty}^{\infty} \hat{f}(R,\omega) e^{i\omega t}\, \mathrm{d}\omega \tag{2}$$

to give

$$\hat{p}_i' = \frac{i\omega_C M_C}{R}\cos\theta \int_{-\infty}^{\infty} \exp[-i(\omega-\omega_C)t]\, \mathrm{d}t$$
$$= \frac{i2\pi\omega_C M_C}{R}\cos\theta\,\delta(\omega-\omega_C) \tag{3}$$

where $\delta(\omega-\omega_C)$ denotes the δ function.

Outer Equation and Its Solution

As mentioned earlier, there is an outer characteristic length, which is much larger than the body length. This length can now be used to rescale the coordinates in the outer region to give

$$X = M_C \bar{x}/\bar{a}, \qquad Y = M_C \bar{y}/\bar{a}$$

With the rescaled coordinates held fixed and letting the Mach number tend to zero, the governing equation reduces to the classical acoustic equation. Its form in the polar coordinates becomes

$$\frac{\partial^2 p_0'}{\partial R^2} + \frac{1}{R}\frac{\partial p_0'}{\partial R} + \frac{1}{R^2}\frac{\partial^2 p_0'}{\partial \theta^2} - \frac{\partial^2 p_0'}{\partial t^2} = 0 \tag{4}$$

where the subscript 0 refers to the perturbed p in the outer region. In view of the inner solution in Eq. (1), the outer solution is assumed to be of the form

$$p_0' = q_0(R,t)\cos\theta \tag{5}$$

On substitution of this expression in Eq. (4), and on application of the Fourier transform, it becomes

$$\frac{\mathrm{d}^2\hat{q}_0}{\mathrm{d}R^2} + \frac{1}{R}\frac{\mathrm{d}\hat{q}_0}{\mathrm{d}R} + \left(\omega^2 - \frac{1}{R^2}\right)\hat{q}_0 = 0 \tag{6}$$

This is the Bessel equation of the first order, whose solution for the outgoing wave is the Hankel function of the second kind and is given by

$$\hat{p}_0' = A H_1^{(2)}(\omega R)\cos\theta \tag{7}$$

where A is the unknown coefficient to be determined by matching.

Matching and Inverse Transform

Equation (7) is to be matched with the inner solution Eq. (3) by the method of asymptotic matching.[14] With the aid of Ref. 16 for $R \to 0$, Eq. (7) reduces to

$$\hat{p}_0' \cong (iA/\pi)(2/\omega R)\cos\theta \tag{8}$$

Comparing this expression with Eq. (3) gives

$$\hat{p}_0' = \pi^2 M_C \omega_C \omega\, \delta(\omega-\omega_C) H_1^{(2)}(\omega R)\cos\theta \tag{9}$$

The inverse transform of Eq. (9) is

$$p_0' = \frac{1}{2\pi}\int_{-\infty}^{\infty} \hat{p}_0' e^{i\omega t}\, \mathrm{d}\omega = \frac{\pi M_C \omega_C}{2}\cos\theta$$
$$\times \int_{-\infty}^{\infty} \omega\delta(\omega-\omega_C) H_1^{(2)}(\omega R) e^{i\omega t}\, \mathrm{d}\omega$$
$$= \frac{\pi M_C \omega_C^2}{2}\cos\theta\, H_1^{(2)}(\omega_C R) e^{i\omega_C t} \tag{10}$$

This expression represents the far-field sound pressure radiated from the oscillating cylinder and is equivalent to the analytical solution of Eqs. (2–69) in Ref. 4. For the purpose of comparison, the denominator in Eqs. (2–69) has to be approximated by its limiting form for a small argument[16] because of the assumption of the small compactness ratio.

Formulation of Problem in Inner Region

Because the flow in the inner region is incompressible, its complex potential is

$$W = \Phi + i\Psi = \sum_{m=1}^{M} \frac{i\gamma_m ds_m}{2\pi}\log(z-z_m)$$
$$+ \sum_{j=1}^{N} \frac{i\Gamma_j}{2\pi}\log(z-z_j) + z \tag{11}$$

where $z = x + iy$ represents a field point in the flowfield; $z_m = x_m + iy_m$ refers to the midpoint in the surface vorticity element s_m, whose vorticity strength per unit length is γ_m; and ds_m is the length of this element (Fig. 1). The symbol $z_j = x_j + iy_j$ refers to the location of Γ_j. The vorticity strengths γ_m and Γ_j are defined to be positive when clockwise in accordance with Lewis's[15] convention. The first group of terms refers to M surface vorticity elements of unknown strengths and the second group to N free vortices of given strengths. The last term denotes the complex potential of the freestream velocity. All quantities are dimensionless and are defined in a similar manner as for Eq. (1). The characteristic length here is the longitudinal length of the body $\bar{L}$, and the characteristic velocity is the freestream velocity $\bar{U}_0$.

The derivative of W with respect to z gives the field velocity components u and v in the x and y directions, as follows:

$$u(x,y) = \sum_{m=1}^{M} \frac{\gamma_m ds_m}{2\pi}\frac{y-y_m}{(x-x_m)^2+(y-y_m)^2}$$
$$+ \sum_{j=1}^{N} \frac{\Gamma_j}{2\pi}\frac{y-y_j}{(x-x_j)^2+(y-y_j)^2} + 1$$
$$v(x,y) = -\sum_{m=1}^{M} \frac{\gamma_m ds_m}{2\pi}\frac{x-x_m}{(x-x_m)^2+(y-y_m)^2}$$
$$- \sum_{j=1}^{N} \frac{\Gamma_j}{2\pi}\frac{x-x_j}{(x-x_j)^2+(y-y_j)^2} \tag{12}$$

The freestream velocity is assumed to be always parallel to the x direction. Thus, the angle of attack of a body is the angle between the x axis and the blade chord.

As the field point x and y approaches the surface point x_m and y_m, Eqs. (12) reduce to Eqs. (13). The solution of this system determines the unknowns γ_m:

$$\frac{1}{2\pi}\sum_{m=1,m\neq n}^{M} \gamma_m ds_m K_b(s_n,s_m) + \gamma_n\left(\frac{1}{4\pi}\frac{ds_n}{R_n} - \frac{1}{2}\right)$$
$$= -\frac{1}{2\pi}\sum_{j=1}^{N} \Gamma_j K_v(s_n,z_j) - \cos\theta_n$$

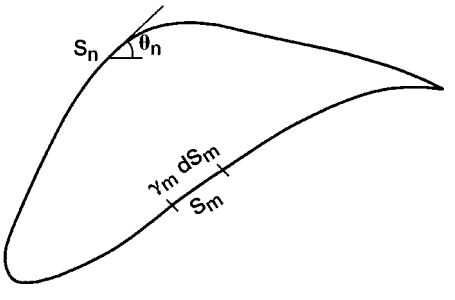

Fig. 1 Surface vorticity elements on a two-dimensional body.

where $n = 1, \ldots, M$,

$$K_b(s_n, s_m) = \frac{(y_n - y_m)\cos\theta_n - (x_n - x_m)\sin\theta_n}{(x_n - x_m)^2 + (y_n - y_m)^2}$$

$$K_v(s_n, s_j) = \frac{(y_n - y_j)\cos\theta_n - (x_n - x_j)\sin\theta_n}{(x_n - x_j)^2 + (y_n - y_j)^2} \qquad (13)$$

Here, $K_b(s_n, s_m)$ and $K_v(s_n, s_j)$ are two influence coefficients representing the tangential velocity components at s_n induced by other vorticity elements and by free vortices, respectively. The symbol R_n is the radius of curvature at s_n and θ_n is the tangential angle (Fig. 1). The second term in the first equation accounts for the self-induced velocity of γ_n at element s_n (Ref. 15).

Equations (13) are a system of M linear equations for M unknowns, which can be solved by any standard method. The Gaussian elimination method was used for every example shown here.

With the quantities γ_m determined, the convective velocities for vortex Γ_k are known and are given by

$$\frac{\mathrm{d}x_k}{\mathrm{d}t} = u_k, \qquad \frac{\mathrm{d}y_k}{\mathrm{d}t} = v_k$$

For a system of N vortices, there are $2N$ such equations whose solutions give the vortex trajectories. A second-order method is used for time evolution from t to $t + \Delta t$:

$$x_k(t + \Delta t) = x_k(t) + \tfrac{1}{2}[3u_k(t) - u_k(t - \Delta t)]\Delta t$$

$$y_k(t + \Delta t) = y_k(t) + \tfrac{1}{2}[3v_k(t) - v_k(t - \Delta t)]\Delta t \qquad (14)$$

At each time step, u_k and v_k must be updated by solving Eqs. (12–14) anew. The time step Δt is generally determined by comparing two solutions, one obtained with Δt and the other with $\Delta t/2$. If the agreement is reasonably good, the time step Δt is chosen; otherwise the process continues. It turned out that $\Delta t = 0.0125$ was adequate for every case in this study, and it is used for most of the computations here. If a vortex comes very close to the blade, the accuracy of Martensen's surface vorticity method may deteriorate as amply demonstrated by Lewis.[15] However, this is not a concern in the present investigation because none will be very near.

Inner Solution and Its Fourier Transform

Unlike an oscillating cylinder, which is always unsteady, the potential flow solution for body–vortex interaction involves a steady part. This part can be neglected because a steady motion generates no sound. Therefore, only the unsteady part of the pressure will be considered. This is accomplished by means of the linearized Bernoulli equation

$$p_i' = p - p_0 = -\frac{\mathrm{D}\phi'}{\mathrm{D}t} \qquad (15)$$

where ϕ' refers to the unsteady part of the velocity potential and $\mathrm{D}/\mathrm{D}t$ is the time rate of change in a coordinate system moving with the undisturbed fluid velocity.

For lifting bodies with temporal loading, vortices will be shed continuously. There are large numbers of mutually interacting vortices in the flowfield, all of which are similar. It is, therefore, possible to use one term to represent the entire group, and Eq. (11) becomes

$$W = \Phi + i\Psi = \sum_{m=1}^{M} \frac{i\gamma_m ds_m}{2\pi} \log(z - z_m) + \frac{i\Gamma_1}{2\pi} \log[z - (t + z_{ct} + z_1)] + z \qquad (16)$$

where z_{ct} denotes the initial location of a vortex, which is either far upstream of the blade or immediately behind the trailing edge for a nascent vortex just being shed. This is invariant with time. The term $t + z_{ct}$ refers to the position of a vortex at time t convected by the freestream velocity $U_0 (U_0 = 1)$ in the absence of the body and is steady. The term z_1 is the perturbed position of the vortex at time t relative to the unperturbed position, $t + z_{ct}$. Thus, only the terms γ_m and z_1 in this equation are time dependent.

After exclusion of the steady part, Eq. (16) becomes

$$W' = \sum_{m=1}^{M} \frac{i\gamma_m ds_m}{2\pi} \log\left[z\left(1 - \frac{z_m}{z}\right)\right] + \frac{i\Gamma_1}{2\pi} \log\left[1 - \frac{z_1}{z}\right] \qquad (17)$$

Expanding this equation for $|z_m/z| \ll 1$ and $|z_1/z| \ll 1$ and defining $z = r\exp(i\theta)$, where θ is the angle of the receiver relative to the positive x axis and $z_m = \delta_m \exp(i\theta_m)$, one obtains

$$W' = \sum_{m=1}^{M} \frac{i\gamma_m ds_m}{2\pi}\left[\log r + i\theta - \frac{\delta_m}{r}\exp[i(\theta_m - \theta)]\right] - \frac{i\Gamma_1}{2\pi}\frac{z_1}{z} + \cdots \qquad (18)$$

in which only the first-order unsteady terms are retained. This equation, as written, is valid for nonlifting bodies only, where the terms involving $\log r$ and θ are zero because, with no circulation around bodies,

$$\sum_{m=1}^{M} \gamma_m ds_m = \oint \left(\frac{\partial\phi}{\partial s}\right) \mathrm{d}s = 0$$

For lifting bodies, the Kutta condition is imposed, resulting in vortex shedding and the cancellation of the singular terms involving $\log r$ and θ in Eq. (18). In an inviscid fluid the circulation must be conserved. Thus, an incident vortex introduced in the upstream is accompanied by a vortex of opposite sense somewhere at infinity. The same argument holds true for the bound circulation for an airfoil at an angle of attack. In other words, Kelvin's circulation theorem must be true for a large closed curve surrounding the whole system in the entire history of the motion. It follows that

$$\Gamma_b + \Gamma_1 + k_2 + k_3 + \cdots = \Gamma_b^{(0)} + \Gamma_1 \qquad (19)$$

In this equation, $\Gamma_b^{(0)}$ is the bound circulation of the blade under an angle of attack without the incident vortex and is a constant. For a symmetric body without the angle of attack, $\Gamma_b^{(0)}$ is zero. Γ_b is the bound circulation at a later time in the presence of vortices, irrespective of the angle of attack because induced velocities can create a local angle of attack. Depending on positions of the incident vortex and the shed vortices, the value of Γ_b changes with time. For a single blade, one vortex is shed after each computational step and is placed at a distance of $\Delta t/2$ directly behind the trailing edge. Thus, the symbols $k_2, k_3, \ldots$, refer to vortices shed sequentially in time. Note that the quantity Γ_1, the strength of the incident vortex, appears on both sides of the equation.

Although the trailing-edge condition in an unsteady flow is still under investigation,[17] imposing it in some form is essential so that the fluid leaves the trailing edge smoothly. For a straight wake, the static pressure at the trailing edge from the upper and lower surfaces must tend to the same value. Gostelow's discussion about this condition, based on Taylor's and Preston's work, can be found in Ref. 18. The circulation theorem, Eq. (19), together with this trailing-edge condition can lead to a unique solution. To implement this procedure, Wilkinson's method 2, stated in Ref. 15, is used.

As mentioned earlier, there is a singularity in Eq. (18) for a lifting body. This singularity can be removed by means of Eq. (19). To this end, Eq. (18) is rewritten as follows, with the shed vortices included:

$$W' = \sum_{m=1}^{M} \frac{i\gamma_m ds_m}{2\pi} \log\left[z\left(1 - \frac{z_m}{z}\right)\right] + \frac{i\Gamma_1}{2\pi} \log\left[1 - \frac{z_1}{z}\right] + \frac{ik_2}{2\pi} \log\left[z\left(1 - \frac{z_2}{z}\right)\right] + \frac{ik_3}{2\pi} \log\left[z\left(1 - \frac{z_3}{z}\right)\right] + \cdots \qquad (20)$$

After the circulation theorem is imposed and the expansion performed, this equation reduces to

$$W' = -\sum_{m=1}^{M} \frac{i\gamma_m ds_m}{2\pi}\frac{\delta_m}{r}\exp i(\theta_m - \theta) - \frac{i\Gamma_1}{2\pi}\frac{z_1}{z} - \frac{ik_2}{2\pi}\frac{z_2}{z} - \frac{ik_3}{2\pi}\frac{z_3}{z} - \cdots$$

By means of the linearizied Bernoulli equation, the unsteady pressure due to the body–vortex interaction in the inner region becomes

$$p_i' = \sum_{m=1}^{M} \frac{\partial \gamma_m}{\partial \tau} \frac{ds_m}{2\pi} \frac{\delta_m}{r} \sin(\theta - \theta_m) + \frac{\Gamma_1}{2\pi r}\left(\frac{Dx_1}{D\tau}\sin\theta - \frac{Dy_1}{D\tau}\cos\theta\right) + \frac{k_2}{2\pi r}\left(\frac{Dx_2}{D\tau}\sin\theta - \frac{Dy_2}{D\tau}\cos\theta\right) + \cdots \tag{21}$$

where r and θ denote, as before, the radial distance and angle from the origin to the observer. The quantity $\partial\gamma_m/\partial\tau$ is the time rate of change of surface vorticity per unit length at a fixed point, whereas $Dx_1/D\tau, Dx_2/D\tau, \ldots$ are the total derivatives, the differences of vortex positions observed in a coordinate system moving at the freestream speed. Because the observer is stationary but vortices are in motion, r and θ will change with time, except those measured from the surface vorticity elements to the observer. However, because interactions become important only when vortices are near the blade, it is, therefore, assumed that these variable r and θ can be approximated by the fixed r and θ from the origin to the observer. The error incurred in this approximation is small because the present concern is with the far-field noise.

It is assumed that one vortex is shed from each trailing edge after each time step. Thus, there will be two or more trails of wakes for a system with two or more blades. The problem of finding a unique solution once again appears. Under the assumption of straight wakes, the trailing-edge condition stated before is valid for each individual blade separately, which implies that one Eq. (19) corresponds to each blade. At first glance, it appears that this procedure decouples blades in the system. The coupling still exists, except that it is now through the application of Wilkinson's method (see Ref. 15), which requires solving simultaneous equations. Some unknowns in these equations are Γ_b in Eqs. (19), which are coupled. A physical interpretation may also lend support to this argument. When blades are far apart, it is reasonable to assume that vortex shedding of one blade is independent, or nearly so, from other blades. As they move closer, shedding remains independent except that the bound circulations are now coupled.

Applying the Fourier transformation to Eq. (21) gives the transformed p_i'

$$\hat{p}_i' = \frac{M_0}{2\pi}\sum_{m=1}^{M}\frac{ds_m\delta_m}{R}\sin(\theta-\theta_m)\int_{-\infty}^{\infty}\frac{\partial\gamma_m}{\partial\tau}e^{-i\omega\tau}\,d\tau + \frac{\Gamma_1 M_0}{2\pi}\left[\frac{\sin\theta}{R}\int_{-\infty}^{\infty}\frac{Dx_1}{D\tau}e^{-i\omega\tau}\,d\tau - \frac{\cos\theta}{R}\int_{-\infty}^{\infty}\frac{Dy_1}{D\tau}e^{-i\omega\tau}\,d\tau\right] + \frac{k_2 M_0}{2\pi}\left[\frac{\sin\theta}{R}\int_{-\infty}^{\infty}\frac{Dx_2}{D\tau}e^{-i\omega\tau}\,d\tau - \frac{\cos\theta}{R}\int_{-\infty}^{\infty}\frac{Dy_2}{D\tau}e^{-i\omega\tau}\,d\tau\right] + \cdots \tag{22}$$

where M_0 is the freestream Mach number and $R = M_0 r$.

Outer Solution, Asymptotic Matching, and Inverse Transform

The proper form of the governing equation in the outer region is the convective wave equation

$$\frac{\partial^2 p_0'}{\partial x^2} + \frac{\partial^2 p_0'}{\partial y^2} - M_0^2\frac{D^2 p_0'}{Dt^2} = 0$$

where $D/Dt = \partial/\partial t + \partial/\partial x$. This equation can be transformed to a form similar to the classical acoustic equation

$$\frac{\partial^2 p_0'}{\partial x'^2} + \frac{\partial^2 p_0'}{\partial y'^2} - \frac{\partial^2 p_0'}{\partial t'^2} = 0$$

by referring x' to $M_0 x$, y' to $M_0 y$, and t' to t and letting $M_0 \to 0$, while holding x' and y' fixed. For instance, the classical acoustic equation was also used by Conlisk and Veley[10] for the noise generation by the motion of vortices over a step. Thus, the governing equation in the outer region in this study is still Eq. (4). The solution of this equation is suggested by the inner solution and is assumed to be

$$p_0' = \sum_{m=1}^{M} p_m(R,t)\sin(\theta_m - \theta) + [p_{1s}(R,t) + p_{2s}(R,t) + \cdots]\sin\theta + [p_{1c}(R,t) + p_{2c}(R,t) + \cdots]\cos\theta \tag{23}$$

where $p_m, p_{1s}, p_{1c}, p_{2s}, p_{2c}, \ldots,$ are functions to be determined. Substituting Eq. (23) into Eq. (4) and performing the Fourier transform results in a set of ordinary differential equations, all of which are of the form of Eq. (6), whose solutions for outgoing waves are the Hankel functions of the second kind. Thus, Eq. (23) becomes

$$\hat{p}_0' = \sum_{m=1}^{M} A_m H_1^{(2)}(\omega R)\sin(\theta - \theta_m) + (A_{1s} + A_{2s} + \cdots)H_1^{(2)}(\omega R)\sin\theta + (A_{1c} + A_{2c} + \cdots)H_1^{(2)}(\omega R)\cos\theta \tag{24}$$

where $A_m, A_{1s}, A_{1c}, \ldots,$ are the unknown coefficients to be determined by matching. For example, A_m are the coefficients for the surface pressure fluctuations, A_{1s} and A_{1c} are for the moving vortex, and the remaining ones are for the shed vortices.

The steps for matching are the same as for the oscillating cylinder. When this is done, Eq. (24) becomes

$$\hat{p}_0' = -\frac{iM_0\omega}{4}\sum_{m=1}^{M} ds_m\delta_m\sin(\theta-\theta_m)H_1^{(2)}(\omega R)\int_{-\infty}^{\infty}\frac{\partial\gamma_m}{\partial\tau}e^{-i\omega\tau}\,d\tau - \frac{i\Gamma_1 M_0\omega}{4}H_1^{(2)}(\omega R)\left[\sin\theta\int_{-\infty}^{\infty}\frac{Dx_1}{D\tau}e^{-i\omega\tau}\,d\tau - \cos\theta\int_{-\infty}^{\infty}\frac{Dy_1}{D\tau}e^{-i\omega\tau}\,d\tau\right] - \frac{ik_2 M_0\omega}{4}H_1^{(2)}(\omega R) \times\left[\sin\theta\int_{-\infty}^{\infty}\frac{Dx_2}{D\tau}e^{-i\omega\tau}\,d\tau - \cos\theta\int_{-\infty}^{\infty}\frac{Dy_2}{D\tau}e^{-i\omega\tau}\,d\tau\right] - \cdots$$

where $k_2, k_3, \ldots,$ refer to the strengths of shed vortices and are zero for nonlifting bodies. This equation, after the inverse Fourier transform, yields the acoustic pressure in the far field

$$p_0' = -\frac{iM_0}{8\pi}\sum_{m=1}^{M} ds_m\delta_m\sin(\theta-\theta_m) \times\int_{-\infty}^{\infty}\omega H_1^{(2)}(\omega R)e^{i\omega t}\,d\omega\int_{-\infty}^{\infty}\frac{\partial\gamma_m}{\partial\xi}e^{-i\omega\xi}\,d\xi - \frac{i\Gamma_1 M_0}{8\pi}\sin\theta\int_{-\infty}^{\infty}\omega H_1^{(2)}(\omega R)e^{i\omega t}\,d\omega\int_{-\infty}^{\infty}\frac{Dx_1}{D\xi}e^{-i\omega\xi}\,d\xi + \frac{i\Gamma_1 M_0}{8\pi}\cos\theta\int_{-\infty}^{\infty}\omega H_1^{(2)}(\omega R)e^{i\omega t}\,d\omega\int_{-\infty}^{\infty}\frac{Dy_1}{D\xi}e^{-i\omega\xi}\,d\xi - \frac{ik_2 M_0}{8\pi}\sin\theta\int_{-\infty}^{\infty}\omega H_1^{(2)}(\omega R)e^{i\omega t}\,d\omega\int_{-\infty}^{\infty}\frac{Dx_2}{D\xi}e^{-i\omega\xi}\,d\xi + \frac{ik_2 M_0}{8\pi}\cos\theta\int_{-\infty}^{\infty}\omega H_1^{(2)}(\omega R)e^{i\omega t}\,d\omega\int_{-\infty}^{\infty}\frac{Dy_2}{D\xi}e^{-i\omega\xi}\,d\xi + \cdots \tag{25}$$

It represents the time history of the far-field sound pressure from far upstream to the end of computation. However, its value becomes

appreciable only in the short interval when the vortex is near the body. Outside of this range, the medium is essentially silent. This property of fast decay can also be seen in the linear theory of Howe.[19]

Discrete Fourier Transform

At first glance, it appears uncertain whether the function in the inverse transform is absolutely integrable because $\omega H_1^{(2)}(\omega R)$ in Eq. (25) approaches $\omega^{1/2}$ as $\omega \to \infty$. However, the fast decay of vortex interaction terms, such as

$$\int_{-\infty}^{\infty} \frac{\partial \gamma_m}{\partial \xi} e^{-i\omega\xi}\, d\xi$$

approaches $1/\omega^2$ at infinity. Thus, the function as a whole is absolutely integrable. The remaining work is to evaluate these integrals numerically by means of the discrete Fourier transform. The accuracy of this procedure has been assessed by comparing to Crighton's analytic results.[7] More details can be found in Ref. 20.

Results and Discussion

In general, for any numerical computation, comparison with experimental data, if available, is essential. However, due to the scarcity of available data, no meaningful comparison seems possible. The only experiment found so far is Booth's.[21] Because his test conditions were very different from the computational ones, only an order-of-magnitude comparison is attainable. Such a comparison was shown graphically in Ref. 20 along with variations between test and computation.

Single Blade

To illustrate the interference mechanism, four examples were computed, two of which are plotted in Fig. 2. As seen, these are merely the far-field acoustic pressures created by a moving vortex passed above a symmetric airfoil (NACA-0012). The only difference between these two is the direction of rotation. A negative vortex (negative when counterclockwise in accordance with Lewis[15]) gives rise to the negative sound pressure, whereas a positive vortex (clockwise rotation) gives rise to the positive sound pressure. The other two examples, not shown, are the counterparts of these two, in which the moving vortex passed below the airfoil. The relationship between the direction of rotation and the sign of the acoustic pressure for these two examples is also the same, except for a slight difference in magnitude. Because the acoustic pressure can either be positive or negative, interference is now attainable.

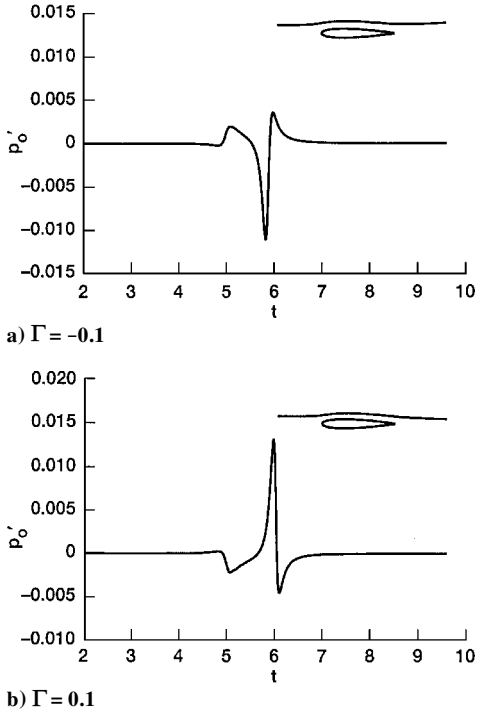

Fig. 2 Time history of sound generation by an NACA-0012 airfoil with a vortex passing above, $x_v = -5.0$, $y_v = 0.1$.

The observer in these four examples is directly above the blade at a distance of 50 chord lengths from the leading edge, which is the origin of the coordinate system, and at 90 deg from the positive x axis (the direction of freestream). The freestream Mach number is 0.2. The initial position of the vortex is 5 chord lengths upstream of the leading edge in the x direction and ± 0.1 chord lengths in the y direction. Because the blade is symmetric, the calculated pressure in Fig. 2a is equivalent to that of a positive vortex passed below the blade with the observer situated below the blade. Note that most of these input parameters remain unchanged throughout the computation. For instance, $r = 50$, $\theta = \pi/2$, $M_0 = 0.2$, and $x_v = -5.0$, except where stated otherwise.

In computations with lifting bodies, wakes always occur due to the local angles of attack brought about by the induced velocities, even though blades are parallel to the freestream. Thus, in the examples of Fig. 2, a part of the solution is the trail of shed vortices (wake), though these are not shown here. (An example of the wake pattern will be shown later.) The presence of the wake causes the vortex trajectories to bend slightly, which can be seen here as well as in later figures.

To present a more complete picture, the directivity pattern for Fig. 2a is shown in Fig. 3a and is seen to be akin to that of a dipole. Figure 3a appears to be symmetric. The reason why this is so is not clear, but it may be due to the circumstances that the body

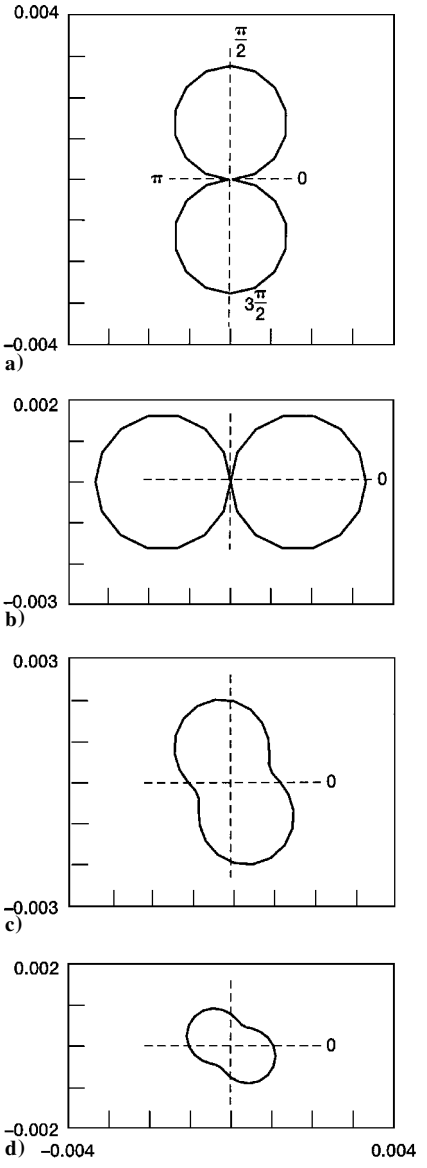

Fig. 3 Directivities for a) Fig. 2a, b) Fig. 6a, c) Fig. 6b, and d) Fig. 7a.

is symmetric and the noise from the wake and the vortex itself is insignificant. The patterns for other three examples are similar and will not be given. The directivities here are the standard polar diagrams with the rms pressures as the radial distances. The sample time for the rms is somewhat arbitrary and was taken to be the range where the sound pressure is visually discernible. The origin of the coordinates is at the leading edge of the blade or at the leading edge of the upper blade, if two blades are present.

Knowing the occurrence of sound pressure of opposite signs, one can take advantage of this property to reduce noise. In an ideal situation, such as that in Fig. 4a, the cancellation is complete and sound is absent. Normally, even if there is no sound produced by the surface, the wake, if it exists, can still generate sound of very low intensity. In this case of total destructive interference, the Kutta condition is automatically satisfied and there is no wake.

For the complete destruction to occur, the blade has to be symmetric and vortices of equal magnitude, opposite sense, and at an equal distance from the blade. They also must pass the blade concurrently. The last condition of concurrent arrival is a very stringent requirement. In other words, the initial positions of these two vortices must be equal horizontally. If, instead of two isolated vortices, there are two streams of closely packed vortices, some of them will probably arrive almost concurrently.

Two vortex paths in Fig. 4a are symmetric with respect to the blade. This is essential for the total destruction; otherwise only a partial destruction is attainable. For instance, Fig. 4b is an example of a partial destruction in which the lower vortex path is 1.5 times farther from the chord than the upper path. The attenuation is still substantial, and it is more evident when the directivity, not shown, is plotted.

Thus far, the strengths of both vortices are equal. This need not be the case and can be shown numerically. In fact, when the strength of the lower vortex in Fig. 4b is reduced, the attenuation increases.

The preceding are two examples with two incident vortices, one on each side. In the following, examples are given with both vortices on the same side of the blade. This is to demonstrate that the primary reason of noise attenuation is the presence of a pair of vortices of opposite sense, regardless of which side of blade. Moreover, the angle of attack need not be zero (Fig. 5a).

The attenuation in Fig. 5a is considerable. This is mainly due to the small separation distance between two vortices and not to the angle of attack. If this distance decreases further, destructive

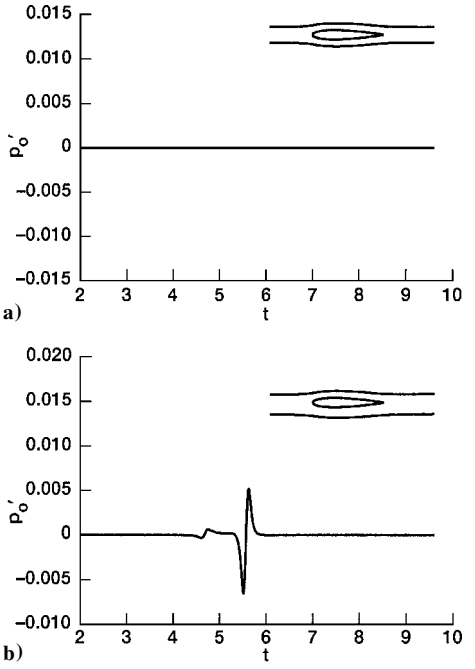

Fig. 4 Time history of acoustic interference: a) complete destruction, $\Gamma = -0.1$ and $y_v = 0.1$, $\Gamma = 0.1$ and $y_v = -0.1$ and b) partial destruction, $\Gamma = -0.1$ and $y_v = 0.1$; $\Gamma = 0.1$ and $y_v = -0.15$. (Upstream positions of these vortices are at $x_v = -5.0$.)

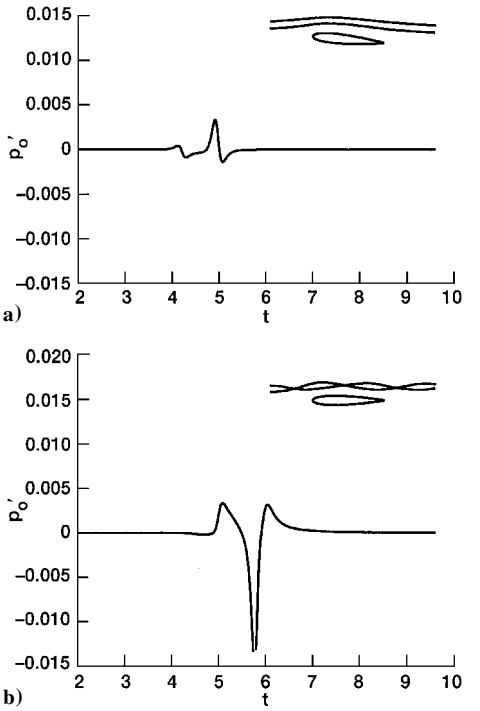

Fig. 5 Time history of acoustic interference: a) partial destructive interference with angle of attack = 5 deg, $\Gamma = 0.1$ and $y_v = 0.03$; $\Gamma = -0.1$ and $y_v = 0.12$ and b) constructive interference, $\Gamma = -0.1$ and $y_v = 0.1$; $\Gamma = -0.1$ and $y_v = 0.18$. (Upstream positions of these vortices are at $x_v = -5.0$.)

interference also will be larger. Another example is the one shown in Fig. 5b, where a pair of vortices of same sense convected by the freestream while rotating about their centroid. Based on the earlier assumption that attenuation is the result of two vortices of opposite sense, one may anticipate a twofold increase in noise in Fig. 5b as compared with Fig. 2a. This is, however, not the case. The reason may be that the blade–vortex interaction for a rotating pair is sufficiently complex that it cannot be explained by the simple addition. The evidence here and elsewhere indicates that a pair of spinning vortices acts somewhat like a single vortex as far as sound production is concerned. (A pair of spinning vortices produces sound by itself,[6] but the intensity is low and cannot be easily discerned here.)

Two or More Blades

Because the present method is not limited to a single body, attention is now given to vortex interactions involving two or more blades with two or more incident vortices. First consider a pair of stacked blades, which is somewhat like a two-dimensional channel. If the gap between them is sufficiently large and there is only one incident vortex moving through the channel, the interference from the other blade is usually small. If there are two incident vortices in the channel as in Fig. 6a, the characteristics of the sound pressure can be rather unexpected. For instance, the sound pressure in Fig. 6a received at $\theta = \pi/2$ is nearly zero. At first glance, one may think that this is a case of complete destructive interference, but one will soon find out that this is not the case after seeing the directivity diagram in Fig. 3b. The overall intensity is actually increased, but the directivity pattern has rotated 90 deg with the minimums in the vertical direction where the signal is received. However, attenuation is still possible by simply shifting the lower vortex upward as illustrated in Fig. 6b. The acoustic pressure in Fig. 6b is decomposed into two parts: one from the upper surface and the other from the lower surface. (In earlier figures, only the total acoustic pressure was plotted.) These two parts are plotted separately, so that the interference can be seen. Because of this interference, the overall intensity is smaller and the directivity pattern is different (Fig. 3c).

A further reduction of sound generation is possible, if two blades form a divergentlike channel as in Fig. 7a. The geometry of the blades is the same as before, except for the outward rotations of

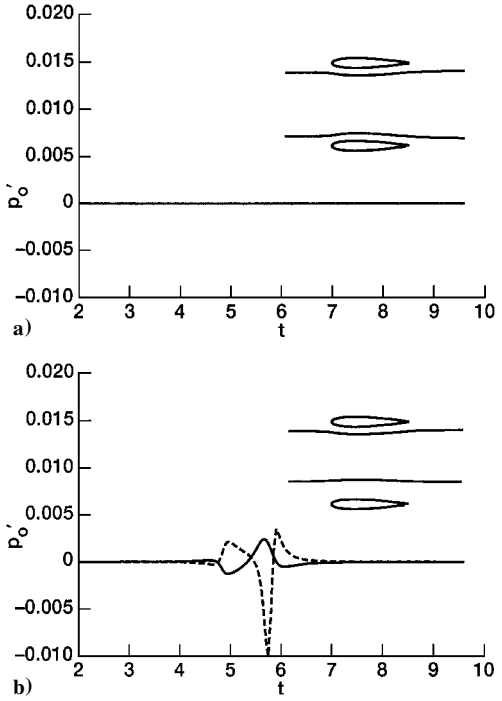

Fig. 6 Time history of acoustic interference by two stacked NACA-0012 airfoils: a) $\Gamma = -0.1$ and $y_v = -0.12$; $\Gamma = 0.1$ and $y_v = -0.88$ and b) decomposition of acoustic pressure, $\Gamma = -0.1$ and $y_v = -0.12$; $\Gamma = 0.1$ and $y_v = -0.72$; ——, acoustic pressure from the lower blade; – – –, acoustic pressure from the upper blade. (Upstream positions of these vortices are at $x_v = -5.0$.)

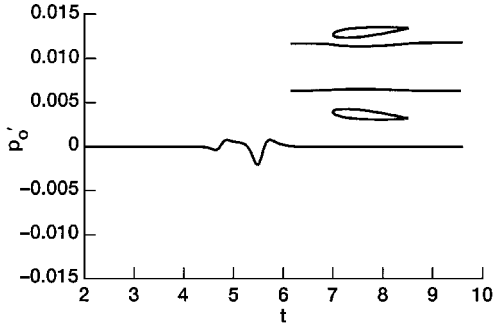

Fig. 7a Time history of sound generation by two blades forming a divergent channel; vortex strengths and upstream positions identical to those in Fig. 6b.

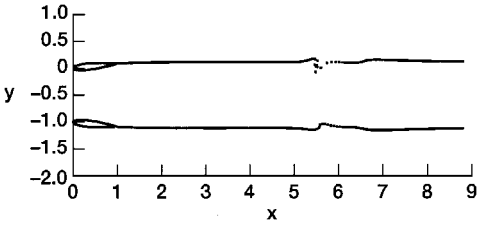

Fig. 7b Snapshot of wakes behind two blades in Fig. 7a.

5 deg. The upstream positions for two incident vortices in this case are also the same as in Fig. 6b. Because two blades rotate outward and the vortex-to-blade distances become larger, reduction in sound intensity is expected. The extent of reduction as shown in Fig. 3d is not foreseen.

Before proceeding any further, it is time to include a snapshot of the wake formation behind the blades. As mentioned earlier, the trailing-edge condition is imposed in computations with lifting bodies. Therefore, wakes, though not plotted, are a part of solutions. The configuration in Fig. 7b should be a part of the insert in Fig. 7a. In the present formulation, and for the convenience of bookkeeping, one

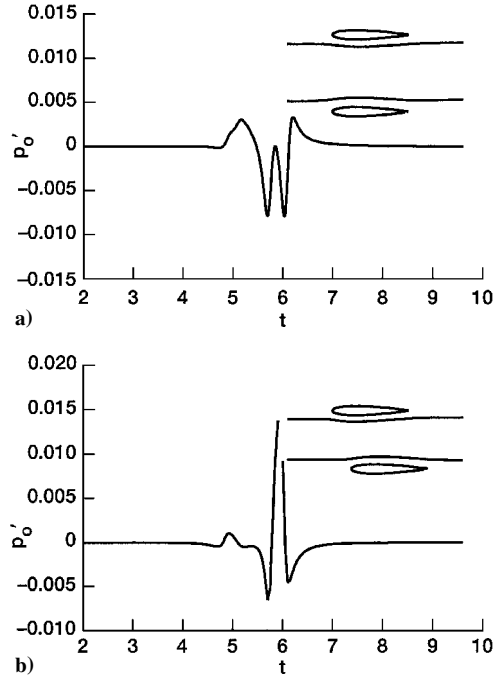

Fig. 8 Two examples of acoustic interference: a) two like-signed vortices, $y_v = -0.12$ and $y_v = -0.88$ ($\Gamma = -0.1$ and $x_v = -5.0$ for both vortices) and b) staggered case, $\Gamma = -0.1$ and $y_v = -0.12$; $\Gamma = 0.1$ and $y_v = -0.63$. (Both upstream positions are at $x_v = -5.0$.)

vortex is shed from each trailing edge at every time step, regardless of its strength. For instance, when the incident vortex is far from the body, the circulation around a large closed curve is essentially invariant, and yet the trailing-edge condition is still imposed and vortices are still shed. The strengths of these vortices are nearly zeros, which manifest as straight lines in Fig. 7b. The curved portions are created while vortices pass near the blades.

The gap between two stacked blades plays also a significant role and cannot be ignored. In general, narrowing the space can reduce the noise level, though generally small, but widening the gap can lead to an increase in noise level, sometimes significantly. It is also possible that repositioning vortex trajectories can lessen the intensity.

As anticipated, a pair of like-signed vortices convected through the space between two stacked blades will cause an increase in intensity as depicted in Fig. 8a, whose directivity is given in Fig. 9a. Even in this case, shifting vortex trajectories is an effective means for noise reduction.

For stacked blades, there is also the effect of staggering (two leading edges are not aligned vertically), which may turn out to be fairly large. This is somewhat equivalent to the nonconcurrent arrival of two vortices. An example is shown in Fig. 8b with its directivity pattern in Fig. 9b. The intensity level is now greatly increased. Besides the usual method of shifting vortex paths, one could reduce the size of the lower blade in this case to lessen the noise. The reduction is only moderate (Fig. 10a).

As the observer moves farther away from the interaction, the received sound is expected to decrease. The relationship is not exactly linear as can be seen in Eqs. (10) and (25). To see this effect, Fig. 10b is included, in which the observer is 100 chord lengths from the origin, as opposed to Fig. 10a, where the observer is 50 chord lengths away.

In the preceding examples, only the blades were stacked, but not the vortices. In the following, we propose to consider two cases of total stacking in the sense that both blades and vortices are stacked, as in Figs. 11, for a two-blade and a three-blade system. To see the difference between these two, Fig. 11a is first calculated, whose directivity is given in Fig. 9c. The noise intensity is higher than that in Fig. 2a, but it is not a twofold increase. The relationship is again not linear, which also can be seen by comparing Figs. 11b and 9d with Figs. 11a and 9c.

Increasing the number of blades and vortices indefinitely results in a cascade. A cascade is an infinite array and cannot be normally

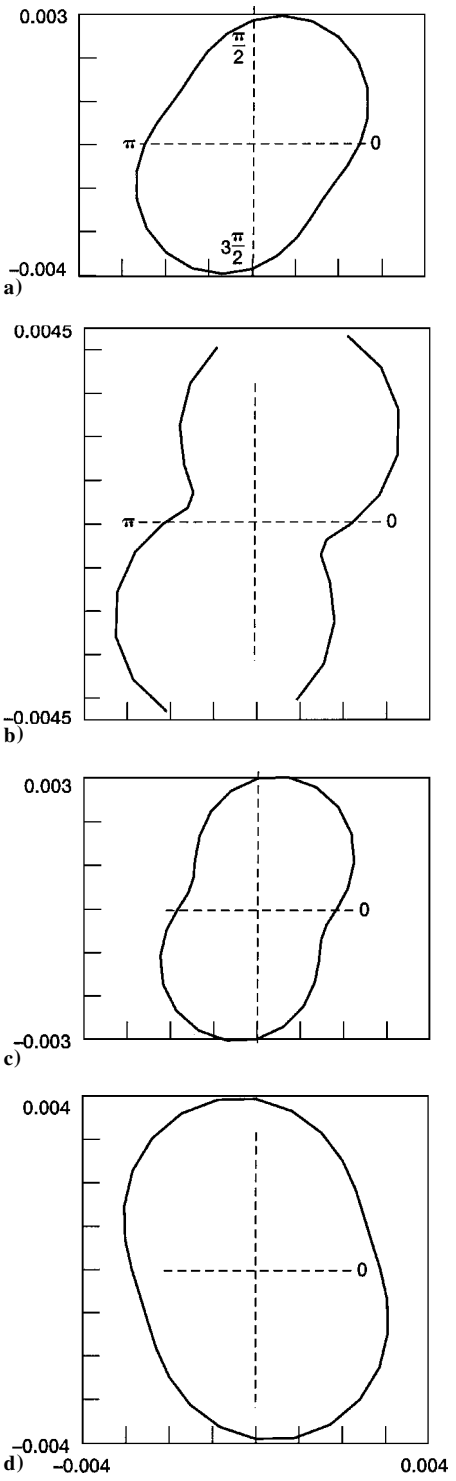

Fig. 9 Directivities for a) Fig. 8a, b) Fig. 8b, c) Fig. 11a, and d) Fig. 11b.

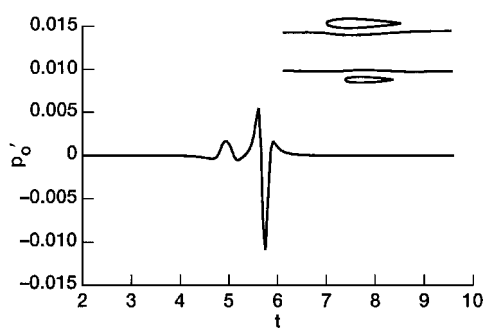

Fig. 10a Vortex strengths and upstream positions identical to those in Fig. 8b, except with a smaller lower blade.

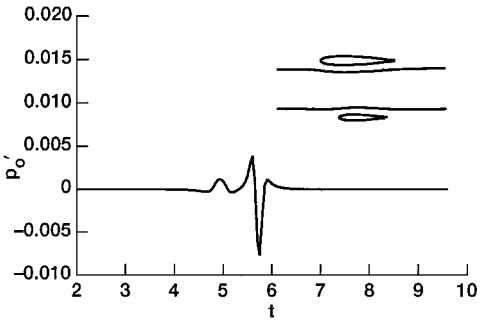

Fig. 10b Conditions identical to Fig. 10a except observer's distance = 100.0 instead of 50.0.

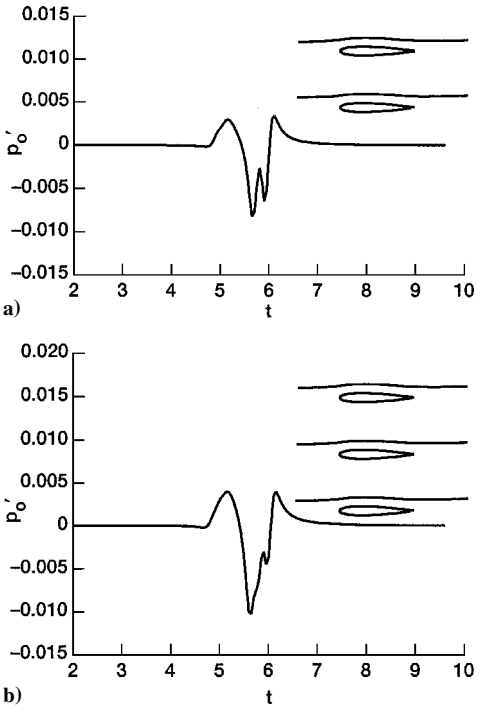

Fig. 11 Comparison of acoustic pressures between two- and a three-blade system. Vortex strengths, upstream horizontal distances, and the space between two blades are identical in both cases ($\Gamma = -0.1, x_v = -5.0$, and space = 0.75): a) $y_v = 0.12$ and $y_v = -0.63$ and b) $y_v = 0.12, y_v = -0.63$, and $y_v = 0.87$.

viewed as a compact body. However, if one agrees with the viewpoint that a single blade in a computational domain, with appropriate periodic conditions, can represent a cascade, a cascade could now be considered a compact body, and the aforementioned formulation can be adopted. It so happens that the sound generation by infinite moving vortices in a cascade is more tractable than those just shown. In fact, an analytic solution can be found. Details are given in Ref. 20.

Nonlifting Bodies

In all earlier cases, only lifting bodies were been studied. It would be of interest to give two examples similar to earlier cases but with nonlifting bodies. In these cases there will not be any wake, and there is no need to impose the trailing-edge condition. However, it was found that the calculated circulation around the body, though small, was not, in general, zero. This discrepancy has to be removed because if the circulation is not zero, the singularity in Eq. (18) will prevail, which will then have a detrimental effect on the sound production. To impose this zero circulation condition, a procedure similar to Wilkinson's method 2 (see Ref. 15) for the Kutta condition was employed.

The first example is similar to Fig. 2a and is shown in Fig. 12a. Note that there is no high peak in the sound production, and the overall intensity is considerably lower than that in Fig. 2a. The second example is similar to that in Fig. 5a. Here, the destructive

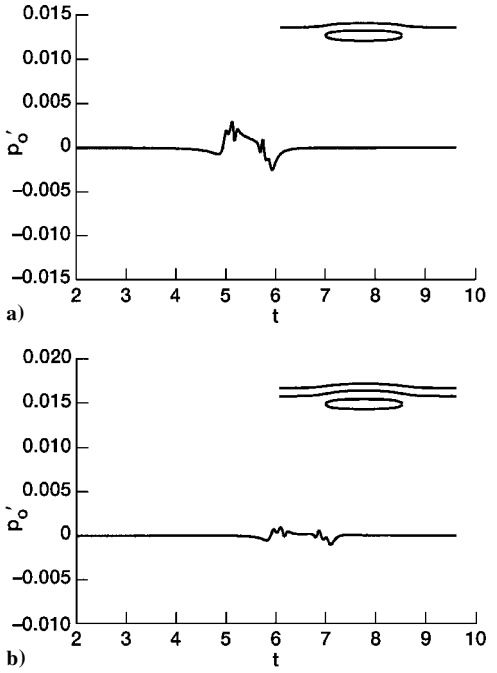

Fig. 12 Time history of acoustic pressure from two nonlifting bodies: a) vortex strength and upstream position identical to those in Fig. 2a and b) $\Gamma = -0.1$ and $y_v = 0.1$; $\Gamma = 0.1$ and $y_v = 0.2$. (Upstream positions are at $x_v = -5.0$.)

interference is obvious and is more effective than that for a lifting body. These two examples seem to indicate that if a lifting body can be replaced by a nonlifting body, the noise production by vortex interaction will be markedly lower. Although not evident, the geometry of this nonlifting body bears similarity to an NACA-0012 airfoil in the sense that it is essentially formed by two front halves of the airfoil. Its thickness is also approximately equal to 12% of the length.

Conclusions

The results of this study may be summarized as follows:

1) A procedure is devised to examine the interaction of multiple bodies with multiple vortices, a prerequisite for sound wave interference.

2) Under various conditions, it is demonstrated that destructive interference is a possible mechanism for suppressing noise production.

3) Based on numerical results, it appears that sound generation by vortex interaction with nonlifting bodies is much lower than that with lifting bodies.

References

[1]Dittmar, J. H., "Interaction of Rotor Tip Flow Irregularities with Stator Vanes as a Noise Source," AIAA Paper 77-1342, Nov. 1977.

[2]Shaw, L. M., and Bolombin, J. R., "Rotor Wake Characteristics Relevant to Rotor–Stator Interaction Noise Generation," *Journal of Aircraft*, Vol. 19, No. 11, 1982, pp. 954–962.

[3]George, A. R., "Helicopter Noise: State-of-the-Art," *Journal of Aircraft*, Vol. 15, No. 11, 1978, pp. 707–715.

[4]Dowling, A. P., and Ffowcs Williams, J. E., *Sound and Sources of Sound*, Wiley, New York, 1983, pp. 40, 61.

[5]Crow, S. C., "Aerodynamic Sound Emission as a Singular Perturbation Problem," *Studies of Applied Mathematics*, Vol. 49, No. 1, 1970, pp. 21–44.

[6]Muller, E. A., and Obermeier, F., "The Spinning Vortices as a Source of Sound," CP-22, AGARD, 1967, pp. 22.1–22.8.

[7]Crighton, D. G., "Radiation from Vortex Filament Method Near a Half Plane," *Journal of Fluid Mechanics*, Vol. 51, Pt. 2, 1972, pp. 357–362.

[8]Davis, S. S., "Theory of Discrete Vortex Noise," *AIAA Journal*, Vol. 13, No. 3, 1975, pp. 375–380.

[9]Hardin, J. C., "Noise Radiation from the Side Edge Flaps," *AIAA Journal*, Vol. 18, No. 5, 1980, pp. 549–552.

[10]Conlisk, A. T., and Veley, D., "The Generation of Noise in Impinging Vortex Motion Past a Step," *Physics of Fluids*, Vol. 28, No. 10, 1985, pp. 3004–3012.

[11]Sen, R., "Vortex-Oscillation Model of Airfoil Side-Edge Noise," *AIAA Journal*, Vol. 35, No. 3, 1997, pp. 441–449.

[12]Hu, F. Q., Martin, J. E., and Hussaini, M. Y., "On Computing Sound Radiation of Temporally Evolving Mixing Layer by Vortex Method and Matched Asymptotic Expansions," AIAA Paper 96-0875, 1996.

[13]Hardin, J. C., and Mason, J. P., "A New Look at Sound Generation by Blade/Vortex Interaction," *Journal of Vibration, Acoustics, Stress, and Reliability in Design*, Vol. 107, No. 2, 1985, pp. 224–228.

[14]Van Dyke, M., *Perturbation Method in Fluid Mechanics*, Parabolic, Stanford, CA, 1975, pp. 80–82.

[15]Lewis, R. I., *Vortex Element Methods for Fluid Dynamic Analysis of Engineering Systems*, Cambridge Univ. Press, New York, 1991.

[16]Abramowitz, M., and Stegum, I. A., *Handbook of Mathematical Functions*, Dover, New York, 1965, p. 360.

[17]Crighton, D. G., "The Kutta Condition in Unsteady Flow," *Annual Review of Fluid Mechanics*, Vol. 17, 1985, pp. 411–445.

[18]Gostelow, J. P., *Cascade Aerodynamics*, Pergamon, Oxford, 1984, pp. 163–166.

[19]Howe, M. S., "The Influence of Vortex Shedding on the Generation of Sound by Convected Turbulence," *Journal Fluid Mechanics*, Vol. 76, 1976, pp. 711–740.

[20]Kao, H. C., "Body–Vortex Interaction, Sound Generation and Destructive Interference," NASA TM-2000-210239, Aug. 2000.

[21]Booth, E. R., "Experimental Observations of Two-Dimensional Blade–Vortex Interaction," *AIAA Journal*, Vol. 28, No. 8, 1990, pp. 1353–1359.

P. J. Morris
Associate Editor